The Meteorological Magazine

January 1990

Steady states in a turbulent atmosphere
Remotely sensed data for wave forecasting

HMSO

Met.O.992 Vol. 119 No. 1410

The Meteorological Magazine

January 1990
Vol. 119 No. 1410

551.513.1:551.58

Steady states in a turbulent atmosphere*

A.A. White
Meteorological Office, Bracknell

Summary

The roles of conceptual models and thought experiments in meteorological dynamics are described for the non-theorist. A survey of steady-state solutions of the equations of fluid motion indicates the value of such solutions in attempts to understand weather and climate anomaly patterns as well as long-term average fields.

1. Introduction

The attainment of a physically consistent understanding of atmospheric dynamics is one of the main aims of meteorology. In addition to being a natural scientific goal, it is clearly relevant to the improvement of forecasting methods. This article describes how a knowledge of possible steady flow states can contribute to the desired understanding of motion on the synoptic scale and larger.

Conceptual models are basic to the understanding of any physical system. Section 2 considers briefly the nature of conceptual models in dynamical meteorology, noting that they may be coarsely divided into steady-state and time-dependent types; an historical perspective proves helpful. Steady flow states are discussed from a theoretical standpoint in sections 3 and 4, some observational results are presented in section 5, and conclusions follow in section 6.

2. Understanding atmospheric dynamics

Since the atmosphere is widely agreed to obey the laws of classical physics, its behaviour is already 'understood' in a very restricted sense. But the atmosphere presents such a wide range of dynamical phenomena, on various space and time scales, that a useful understanding must deal with each phenomenon and its relationship to the others.

2.1 Conceptual models and thought experiments

Conceptual models consist of the notions we have about the phenomena which occur in the atmosphere. They are the building blocks of our understanding of atmospheric behaviour. They are based on observational experience, on a general knowledge of physics, and on results of controlled experiments. The controlled experiments may be actual laboratory experiments (see, for example, Hide 1988), or numerical experiments, or — as will be emphasized here — they may be *thought experiments*: theoretical analyses of the behaviour of an idealized atmosphere under precisely defined conditions. (Narrower definitions are perhaps more usual. Here it is convenient to consider as thought experiments even those theoretical analyses which involve lengthy and detailed mathematics.)

Conceptual models should be flexible structures, for new observations or controlled experiments may reveal inadequacies which suggest their revision (or indeed rejection). Hoskins (1983) discusses further the importance of evolving conceptual models and their relationship with observations and various experimental results.

2.2 Steady-state and time-dependent aspects of atmospheric behaviour

The atmospheric phenomena listed in Table I are divided into possible quasi-steady and time-dependent categories. Such a subdivision depends on tacit choices of a discriminating time scale τ (say) with respect to

* Based on a colloquium given at the Meteorological Office on 22 February 1989.

Table I. A possible division of selected atmospheric phenomena into quasi-steady and time-dependent categories (see text for discussion of the arbitrariness of this division)

Quasi-steady	Time-dependent
Climatological averages	Day-to-day weather changes
Climate anomalies	'Low frequency variability'
Blocking and other weather anomalies lasting up to several weeks	Quasi-biennial oscillation
	El Niño/Southern Oscillation

which quasi-steadiness or time-dependence is to be judged. The categorization of Table I is thus not unique — the same phenomenon may be viewed as quasi-steady or time-dependent according to the choice of τ.

For example, the blocking phenomenon (see Shutts 1987a) may be considered as quasi-steady in relation to an advective time scale L/U, where L and U are synoptic space and velocity scales in the horizontal; note that $L = 1000$ km and $U = 10\ \mathrm{m\ s^{-1}}$ give $L/U \approx 1$ day. But since blocking lasts for only a few weeks, at most, it might also be considered as a natural variability on that time scale. This duality may be recognized to some extent in many atmospheric phenomena.

A steady-state emphasis suggests conceptual models based on steady solutions of the governing equations, while a time-dependent emphasis suggests models based on initial-value problems. The thought experiments in the two cases are thus essentially different. An initial-value problem asks what happens if chosen field patterns are set up at an initial time $t = 0$. A steady-state problem seeks the field patterns for which *nothing* happens when $t > 0$ — the initial state persists.

Since most phenomena have elements of both steadiness and time dependence, conceptual models which emphasize one aspect are likely to give useful (if incomplete) pictures. Putting the different models together can lead to a balanced understanding of the real phenomena.

2.3 Ancient and modern views of the atmosphere's general circulation

The working and interplay of steady-state and time-dependent models may be further elucidated by considering the history of general circulation theory up to about 1970. Some milestones are indicated in Table II. Early theories — up to about 1900 — stressed steady-state aspects, attempting to explain the observed time-averaged circulation directly in terms of the time-averaged distribution of diabatic heating and cooling. A typical example is the circulation pattern proposed by Ferrel (1856) and shown in Fig. 1. The pioneering meteorologists of the day were well aware of the variability of atmospheric flow, especially outside the tropics, but they considered that it did not play a

Table II. Some milestones in general circulation theory (for detailed references see Lorenz 1967)

Date	Scientist	Summary of contribution
1686, 1735	Hadley	Solar heating drives a thermally direct symmetric circulation; zonal component of Coriolis force.
1856	Ferrel	Thermally indirect circulations possible; meridional component of Coriolis force.
1900, 1902	Bigelow	Mid-latitude cyclone/anticyclone systems carry large poleward heat fluxes.
1921	Defant	Mid-latitude motion may be regarded as large-scale turbulence.
1926	Jeffreys	Cyclone/anticyclone systems carry important meridional fluxes of angular momentum as well as heat.
1947	Charney	Instability of baroclinic westerly currents demonstrated.
1949	Eady	

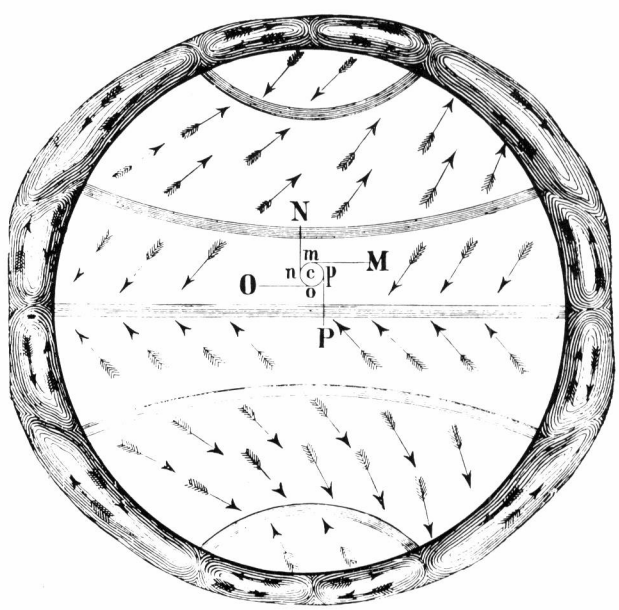

Figure 1. The atmosphere's general circulation according to Ferrel (1856). Arrows indicate the proposed time averaged flow. (Letters M, m, etc. relate to Ferrel's analysis of the forces to which moving air parcels are subject.)

significant part in determining the time-averaged state of the atmosphere. This was a reasonable view to adopt until the need for a more complex picture became clear.

At the turn of the twentieth century it began to be appreciated that the transient cyclones and anticyclones of the extratropics play a key role in the regional heat and momentum budgets of the atmosphere, and hence that the effects of such time-dependent phenomena cannot be omitted from a reliable conceptual model of the time-averaged circulation. The self-contained steady-state models of the eighteenth and nineteenth century thus gave place to steady-state models in which the effects of transient motion played a conspicuous part.

Interest in time-dependent models of transient motion consequently increased, and their study was given added impetus in the late 1940s by Charney's and Eady's instability analyses — *thought experiments* which showed that a baroclinic westerly current could be unstable to wave-like perturbations (Charney 1947, Eady 1949). Theories of transient eddy parametrization (Green 1970) and geostrophic turbulence (Charney 1971) marked the continuation of this trend.

Scientific understanding of atmospheric behaviour undoubtedly increased as a result of the emphasis on time-dependent phenomena which the twentieth century brought. However, it has been widely recognized in recent years that steady-state conceptual models can give useful insight into other atmospheric phenomena besides the long-term average general circulation. Blocked circulation types, other weather anomaly patterns, and climate anomaly patterns are the most promising candidates. The thought experiments which underlie the relevant steady-state models are considered in sections 3 and 4.

Two caveats should be noted about the brief account of general circulation theory given in this section. Table II represents, of course, only a very abridged and selective history; Lorenz (1967) and Pearce (1985) give thorough surveys. Also, though the emphasis in theoretical studies during the 1950s and 1960s was mainly on time-dependent conceptual models and thought experiments, much important work on steady-state models of various phenomena was done too. See, for example, Charney and Eliassen (1949) and Smagorinsky (1953).

3. Steady flow states

The non-divergent barotropic vorticity equation (BVE) is well known as a good qualitative description of atmospheric motion at upper tropospheric levels, and it provides a convenient vehicle for a discussion of steady flow states. Attention is limited to solutions of the complete non-linear equation, so that no restriction to small amplitude disturbances is necessary.

With a vorticity forcing term F the BVE reads

$$\left(\frac{\partial}{\partial t} + \mathbf{v}.\nabla\right)q = F. \qquad (1)$$

The horizontal relative velocity $\mathbf{v}$ and absolute vorticity q are defined in terms of a streamfunction ψ as

$$\begin{aligned} \mathbf{v} &= \mathbf{k} \times \nabla\psi, \\ q &= \nabla^2\psi + f. \end{aligned} \qquad (2)$$

Here $\mathbf{k}$ is unit vector in the local vertical, $\times$ indicates the vector product, ∇ is the horizontal gradient vector operator and ∇^2 is the corresponding Laplacian operator; f is the Coriolis parameter $2\Omega\sin\phi$ (ϕ = latitude, Ω = earth's rotation rate).

Equation (1) governs the time evolution of $\nabla^2\psi$ (and hence of ψ) in terms of the advection of absolute vorticity and the forcing F. Forced solutions satisfy equation (1) with $F \neq 0$, while free solutions require $F = 0$. Steady solutions obey $\partial/\partial t = 0$, and thus represent flow patterns which are stationary relative to the rotating earth. (A wider definition of steadiness — which would complicate the discussion — would require only that the flow pattern be stationary relative to some uniformly rotating coordinate frame and not necessarily the earth's.)

3.1 Steady free flows

When $F = \partial/\partial t = 0$, equation (1) reduces to

$$\mathbf{v}.\nabla q = \mathbf{k}.(\nabla\psi \times \nabla q) = 0. \qquad (3)$$

The horizontal flow $\mathbf{v}$ is everywhere parallel to the contours of constant absolute vorticity q, or, in other words, the contours of constant q are everywhere parallel to the streamlines.

Geostrophically balanced zonal flows obviously satisfy equation (3), but a very wide range of more complicated solutions exists. This fact is of great meteorological importance. Equation (3) is obeyed if there is a functional relation between q and ψ:

$$q = \nabla^2\psi + f = S(\psi). \qquad (4)$$

The function $S(\psi)$ is known as the signature of the free flow. Any reasonable function may be chosen, but equation (4) is most easily solved for ψ when S is linear in ψ, and naturally this case has received the most attention.

3.1.1 Stationary Rossby waves

Suppose that $S(\psi) = -\mu\psi$, where μ is some constant. Then equation (4) can be written as

$$\nabla^2\psi + \mu\psi = -2\Omega\sin\phi. \qquad (5)$$

The eigenfunctions of the horizontal Laplacian operator ∇^2 are obviously relevant to the solution of equation (5). On a sphere, they are the surface harmonics $P_n^m(\sin\phi)\cos(m\lambda+\epsilon)$ where λ = longitude, ϵ is an arbitrary phase factor and the integers m and n are the rank and

degree of the associated Legendre polynomial P_n^m. The choice $\mu = n(n+1)/a^2$, where 'a' is the radius of the sphere, yields a solution of equation (5) consisting of a simple 'solid rotation' zonal flow and a surface spherical harmonic:

$$\psi = -a^2\omega\sin\phi + AP_n^m(\sin\phi)\cos(m\lambda+\epsilon), \quad (6)$$

where

$$\omega = \frac{2\Omega}{(n+2)(n-1)}$$

If $m \neq 0$, the spherical harmonic part of equation (6) represents the spatial structure of a Rossby-Haurwitz wave (or Rossby wave, for short). Its amplitude A is arbitrary. The zonal flow included in the solution is simply that solid rotation which brings the Rossby wave to rest relative to the earth. (The singular case n=1 is well understood but will not be discussed further.)

Various extensions of the solution to equation (6) may be made (see Ertel (1943), Craig (1945) and Neamtan (1946); equation (6) is Ertel's 'specific solution'.) For example, the single Rossby wave in equation (6) may be replaced by any linear combination of waves having the same degree (or total wavenumber) n; so different zonal wavenumbers $m (\leqslant n)$ may be present. Zonal flows having P_n^0 streamfunction structure are also permitted.

Quite complicated steady, free solutions of the BVE thus exist. Fig. 2 shows the hemispheric streamfunction field of a solution composed of a solid rotation zonal flow and Rossby waves of degree n = 6. The signature $q = S(\psi)$ is shown in Fig. 4(a). An infinity of related solutions may be obtained by changing the amplitudes of the constituent Rossby waves; each member of the family has a signature having the same slope $dS/d\psi$.

Similar solutions of the three-dimensional quasi-geostrophic equations (QGEs) are readily constructed (Kuo 1959, Mitchell and Derome 1983, White 1986). The general functional relationship is now

$$Q = S(\psi,z)$$

in the rest frame of the wave, where z is the vertical coordinate and Q the quasi-geostrophic potential vorticity. An interesting example is the neutral, equivalent barotropic mode which is a finite amplitude, long-wave solution of Charney's baroclinic instability problem (see Held *et al.* 1985).

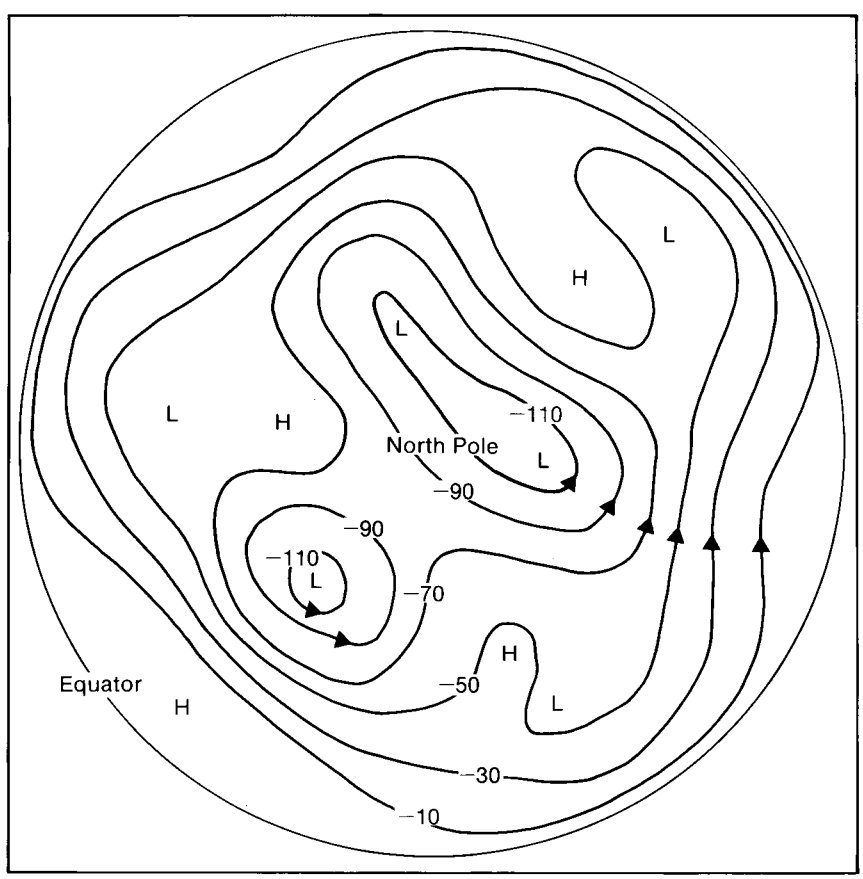

Figure 2. Streamfunction pattern of a multiple Rossby wave solution of the barotropic vorticity equation on a hemisphere. (Distance from north pole is proportional to co-latitude.) The solution is composed of a solid rotation zonal flow and spherical harmonics having n = 6 and m = 1, 3, 5. Arrows indicate direction of flow. Contour interval is 20 in units of $10^{-2} \times \Omega a^2/28$, where 'a' is the earth's radius; this unit corresponds to a geopotential height difference of about 1 dam at latitude 45°N (assuming geostrophic balance). In the same units the amplitudes of the constituent Rossby waves are 15, 25 and 6 for m = 1, 3 and 5; the phases of the m = 1 and m = 5 waves relative to that of the m = 3 wave are $-\pi/4$ and π.

3.1.2 Modons

The Rossby waves presented in the previous section are non-localized, global solutions of the BVE. Global solutions whose spatial variation is essentially localized also exist, including those often referred to as *modons*. Modons consist of interior and exterior regions in which the function $S(\psi)$ takes different forms; continuity conditions are applied at the boundary separating the two regions. In the simplest cases (see Stern 1975 and McWilliams 1980) plane geometry is assumed, the functions $S(\psi)$ are linear, the boundary is circular and the interior streamfunction has dipole form. The flow in the exterior is predominantly zonal. A typical streamfunction field, taken from Butchart *et al.* (1989), is shown in Fig. 3, and the $S(\psi)$ signature — two straight lines — is illustrated in Fig. 4(b).

The amplitude of a modon is not arbitrary but is related in a complicated way to the radius of the boundary and to various other parameters of the system. Certain conditions have to be obeyed by the far-field zonal flow; see, for example, Haines and Marshall (1987). Nevertheless, modons represent a very wide class of possible solutions of the BVE and related equations. Various similar solutions, and some important modifications, have been analyzed in spherical geometry by Verkley (1984, 1987); see also Tribbia (1984).

3.2 Steady forced flows

The free flows discussed in section 3.1 might appear to be meteorologically inapposite precisely because they are free — the forcing F vanishes everywhere. To underpin conceptual models of quasi-steady flows in the real atmosphere it is helpful also to consider steady, forced solutions of the BVE:

$$\mathbf{v}.\nabla q = \mathbf{v}.\nabla(\nabla^2\psi + 2\Omega\sin\phi) = F. \qquad (7)$$

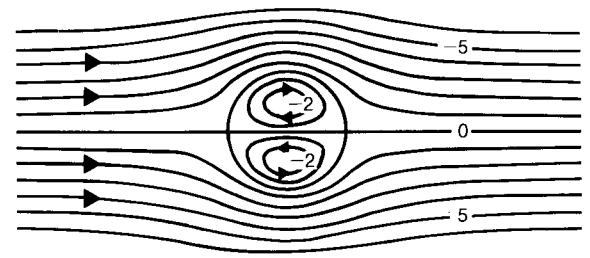

Figure 3. Streamfunction pattern of an equivalent barotropic modon in westerly flow. Units are 10^7 m^2 s^{-1}; arrows indicate direction of flow. From Butchart *et al.* (1989).

3.2.1 Exact solutions

As is well known, any reasonable streamfunction field ψ will be a solution of equation (7) if the forcing F takes an appropriate form: to find F, simply substitute the desired ψ into equation (7) (using equation (2))! Reversing the procedure is generally much more difficult, but it is straightforward if F has certain special properties — indeed, families of solutions of the BVE and of the QGEs may be obtained with wave amplitude as parameter (Derome 1984, Shutts 1987a). The important case in which $F = \mathbf{v}.\nabla h$ (where h represents orography) can clearly be dealt with, but the problem is generally not susceptible to analytical solution when F depends on ψ in such a way that the energetics are non-trivial.

3.2.2 Nearly free flows

In reality, the forcing F is the residual of terms representing various processes, each with its own spatial variation or dependence on ψ. For example, if ψ is a time-averaged streamfunction, F will represent transient eddy vorticity flux convergences as well as frictional dissipation (see, for example, Shutts (1983)). If these processes were in balance everywhere then F would

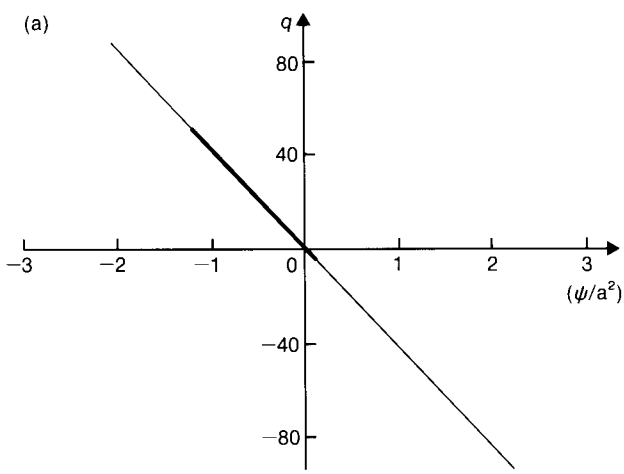

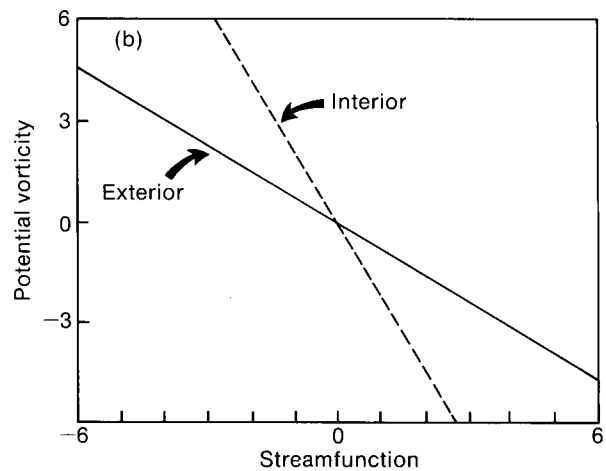

Figure 4. (a) The $q = S(\psi)$ signature (see equations (2) and (4)) of the Rossby wave solution shown in Fig. 2 (bold line), and the remainder of the line (thin) which contains the signatures of all members of the same family of solutions — see text. Both q and ψ/a^2 are plotted in units of $\Omega/28$. (b) The signature of the equivalent barotropic modon shown in Fig. 3. Potential vorticity is here defined as the vorticity relative to the Coriolis parameter on the axis of the flow, plus a term (linear in the streamfunction) which represents the equivalent barotropic character of the flow. Units are 10^7 m^2 s^{-1} for streamfunction and 9×10^{-6} s^{-1} for potential vorticity.

vanish and ψ would be a steady free state; the possibility of analogous states being attained in baroclinic models has been discussed by Mitchell and Derome (1983), Shutts (1987b) and Marshall and So (1989). More generally, systems which are close to a free state, but do not necessarily attain it, may be treated by regarding the time-averaged flow as free at zero order in some suitable parameter and examining the modifications required at first order by the residual forcing F. Thus, with δ as the (small) parameter, and

$$\mathbf{v} = \mathbf{v}_0 + \delta\mathbf{v}_1 + \delta^2\mathbf{v}_2 + \ldots ,$$

$$q = q_0 + \delta q_1 + \delta^2 q_2 + \ldots ,$$

$$F = \delta F_1 ,$$

equation (7) becomes

$$\mathbf{v}_0.\nabla q_0 = 0 \qquad \text{at zero order}$$

and $$\mathbf{v}_0.\nabla q_1 + \mathbf{v}_1.\nabla q_0 = F_1 \qquad \text{at first order.}$$

The deviation from free flow is sufficiently small in many real systems to enable useful and detailed models to be constructed in this way. An important aspect of the analysis is that a solvability condition arises which constrains the signature (q_0=$S_0(\psi_0)$) of the zero-order free flow in terms of parameters describing the residual forcing.

This 'nearly free' analysis, which is currently the subject of much study, has been used in oceanographical or meteorological contexts by Niiler (1966), Rhines and Young (1982), Pierrehumbert and Malguzzi (1984), Marshall and Nurser (1986) and others.

4. Discussion

It is important to make clear how the solutions surveyed in section 3 guide the development of conceptual models of quasi-steady flow patterns in the atmosphere. All the solutions are global in the sense that they are defined in an entire geometric region (such as the surface of a sphere). This is so even in the case of modons, although most of their spatial variation is localized. The main significance of such global steady states is not that they could conceivably occur in the real atmosphere, rather they should be regarded as mathematical embodiments of the physical principle that time evolution may be very slow in regions in which the fields adopt certain patterns. In a way, it is a bonus that simple global solutions such as those described in section 3 can be constructed.

In order to illustrate this fundamental point further, let us consider the stationary Rossby waves of section 3.1.1. Only a special sub-set of streamfunction fields — albeit an infinite one — can be expressed solely in terms of spherical harmonics having the same degree (and a solid rotation component). Arbitrary initial conditions applied to the BVE must therefore be expected to evolve through the advection terms in equation (1), with transfer of energy (and error) between different spatial scales. The message of the steady global solutions is that the evolution may be much slower than the formal advection time L/U would suggest, and that it will be particularly slow in regions where the flow approaches ideal stationary Rossby wave form.

Various other aspects or extensions of the solutions are of interest and will be briefly discussed.

4.1 Accessibility

That states similar to the idealized solutions are accessible from reasonable initial conditions has been demonstrated in many cases by numerical integrations of the BVE or QGEs. See, for example, Shutts (1983), Mitchell and Derome (1983), Hou and Farrell (1986) and Haines and Marshall (1987).

4.2 Stability

General theoretical criteria are usually not helpful in attempts to demonstrate the stability of non-zonal flows to perturbation. Furthermore, the question of the stability of time-averaged flows is beset by problems of interpretation (see Andrews (1984) and references therein). However, the numerical integrations just cited in section 4.1 indicate the effective stability of many steady flow states — although some cases remain to be investigated. Instability on a fairly short time-scale has been demonstrated for some modon-like structures, but others are far more resilient to perturbation (Verkley 1988). Rossby waves become unstable when certain critical amplitudes are exceeded (Baines 1976).

4.3 Variational principles

Important connections, which can only be hinted at here, have been demonstrated between steady, free flows and extremal principles (such as enstrophy minimization at constant energy). See Stern (1975), Bretherton and Haidvogel (1975), Young (1987) and Verkley (1988).

4.4 Steady solutions of the hydrostatic primitive equations

As has been noted, the solutions of the BVE described in section 3 have many counterparts in the QGEs. Except for zonal flows in geostrophic balance, however, very few steady, free solutions of the nonlinear hydrostatic primitive equations (HPEs) are known. (The HPEs form the basis of most modern weather prediction and climate simulation models and are perhaps the most important approximate dynamical formulation used in meteorology.) Zhang *et al.* (1986) describe solutions corresponding to Rossby waves which were derived by applying an iterative numerical method to the HPEs.

In some respects the existence of steady HPE solutions is a side issue, since the known steady solutions

of the BVE and QGEs indicate that *slowly-evolving* states exist in flow governed by the HPEs. The BVE and QGEs are, after all, good approximations to the HPEs for motion on the synoptic scale.

Nevertheless, it is useful in data analysis to be able to define the problem in the HPEs, even if its mathematical solution is generally difficult, for the extent to which real flows approach steady, free states may then be studied. A way of doing this was pointed out to the author by Dr D.G. Andrews in 1985, and an application to atmospheric data will be described in the next section. The analytical details will not be given here. The key result is that a steady, free state of the HPEs yields a functional relationship between Ertel's potential vorticity, P, on any surface of constant potential temperature, θ, and the streamfunction Ψ of the quantity $\mathbf{v}\,\partial p/\partial\theta$ on the same surface. Here $\mathbf{v}$ is the horizontal flow, p = pressure and P is given by

$$P = -(f + \zeta_\theta)\frac{\partial\theta}{\partial p}$$

in which ζ_θ is the relative vorticity evaluated on a potential temperature surface. (See Hoskins *et al.* (1985) for a full account of the properties and usefulness of P.) Thus

$$P = \mathrm{S}(\Psi,\theta)$$

(where S is the signature) in steady, free flow governed by the HPEs.

The approach to such a state in a real flow may be gauged by plotting against each other the values of P and Ψ obtained from a chosen potential temperature surface. Such 'scatter diagrams' indicate the extent of deviation from a functional relation, and hence allow the departure of the flow from steady, free form to be appraised; for an ideal free, steady flow the scatter diagram of course gives the signature (at the chosen value of θ). Read *et al.* (1986) describe the use and interpretation of similar diagrams within the confines of quasi-geostrophic dynamics.

5. An observational study

Fig. 5(a) shows the fields of Ertel potential vorticity P and the streamfunction Ψ computed from 1985/86 winter (December, January, February) mean fields interpolated to the 330 K potential temperature surface. (This surface is in the troposphere in low latitudes, crosses the tropopause in middle latitudes and remains in the stratosphere in high latitudes.) Initialized ECMWF data formed the basis for the calculations, which were carried out by Dr N. Butchart.

The contours of Ertel potential vorticity tend to be concentrated in high latitudes, and the contours of streamfunction in lower latitudes. This behaviour is to be expected given the inverse role of $\partial p/\partial\theta$ in the two fields (see section 4.4) and the increased static stability in the stratosphere. Nevertheless, the contours of the two

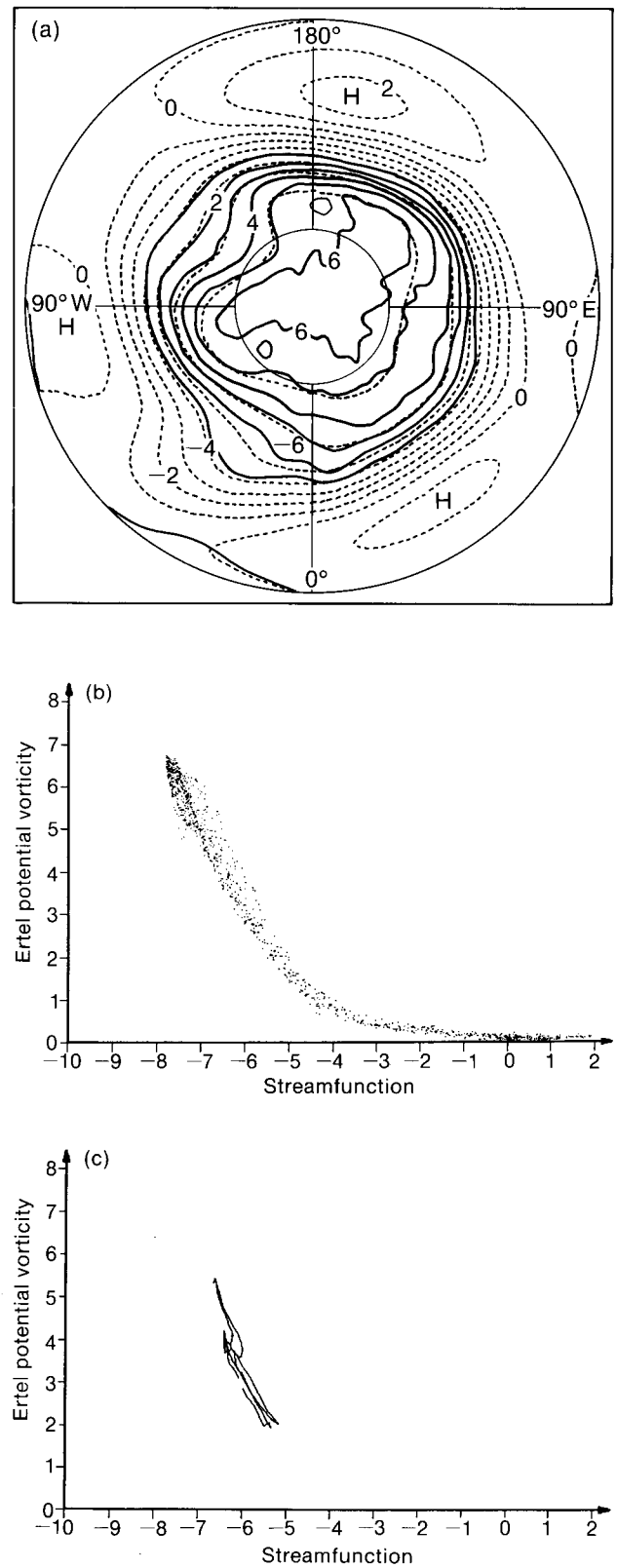

Figure 5. (a) Northern hemisphere fields of Ertel potential vorticity P (full lines) and streamfunction Ψ (broken lines) on the 330 K potential temperature surface, computed from mean initialized ECMWF data for winter 1985/86. Units 10^{-6} m^2 s^{-1} K kg^{-1} for P, 10^{-10} N K^{-1} s^{-1} for Ψ. (b) Scatter diagrams composed of P and Ψ values from all northern hemisphere data grid-points. (c) 'Zonal transect' consisting of P and Ψ values from all data grid-points lying along latitude 40° N. Values from adjacent longitudes have been joined by straight lines.

fields clearly tend to run parallel to one another. The closeness to a functional relationship between P and Ψ is brought out by the scatter diagrams shown in Figs 5(b) and 5(c): Fig. 5(b) contains the P and Ψ values from all data grid-points in the northern hemisphere, while Fig. 5(c) shows the values only from points lying on latitude 40° N. (Zonal transects such as Fig. 5(c) reveal the extent to which hemispheric plots such as Fig. 5(b) reflect merely the latitude variations of the Coriolis parameter and the zonal mean static stability.)

Some departure from free form is, of course, inevitable in real flows. There is also some slight uncertainty in the interpretation of the results shown in Fig. 5 since the plotted quantities are calculated from the seasonal mean flow and pressure fields (rather than being the actual seasonal means of P and Ψ). However, the typical results shown in Fig. 5 strongly suggest that free, steady states constitute good zero-order models of the seasonal mean flow; Fig. 5(c) is a particularly reliable indicator. This is precisely the position which quasi-geostrophic theory is now equipped to exploit (see section 3.2).

6. Conclusions

Approximate forms of the equations governing atmospheric motion possess a wide variety of large amplitude, steady solutions. The essence of these solutions is the ability of the flow to adopt patterns in which a vorticity (or potential vorticity) field is nearly similar in form to a streamfunction field. Evidence of such configurations in seasonal mean data has been presented. Butchart *et al.* (1989) find similar behaviour in 5-day mean fields in a blocking episode: they offer persuasive evidence of the characteristics of the modon solutions of the barotropic vorticity equation which were noted here in section 3.2. It remains to be seen whether other anomaly patterns approach steady, free states and whether their signatures will afford useful characterizations.

Although the atmosphere is obviously a time-varying system, a full understanding of its behaviour should take into account its ability to settle into slowly varying states (usually with transient motion superimposed). In other words, conceptual models should be based on the results of searches for steady states as well as on the results of initial value problems. By their very nature, slowly varying states will contribute disproportionately to long-term average statistics.

Time variability and quasi-steadiness reflect different possible conditions of (potential) vorticity advection. At the extreme of maximum time-variability, the advection is comparable in magnitude with the product of a typical horizontal velocity U and a typical vorticity gradient; time variation occurs on the advective time scale L/U (L being a typical horizontal length scale) and energy and error are transferred between different scales of motion. At the opposite extreme the advection vanishes (although the fields may have complicated form) and there is no time variation or transfer of properties between different scales. Evolution on time scales greater than L/U should therefore be an expected property of large-scale atmospheric flow, whether or not it is regarded as a form of turbulence. Perhaps a slowly varying substructure should be considered as an intrinsic part of the turbulence.

References

Andrews, D.G., 1984: On the stability of forced non-zonal flows. *Q J R Meteorol Soc,* **110**, 657–662.

Baines, P.G., 1976: The stability of planetary waves on a sphere. *J Fluid Mech,* **73**, 193–213.

Bretherton, F.P. and Haidvogel, D.B., 1976: Two-dimensional turbulence above topography. *J Fluid Mech*, **78**, 129–154.

Butchart, N., Haines, K. and Marshall, J.C., (1989): A theoretical and diagnostic study of solitary waves and atmospheric blocking. *J Atmos Sci*, **46**. To appear.

Charney, J.G., 1947: The dynamics of long waves in a baroclinic westerly current. *J Meteorol*, **4**, 135–162.

—, 1971: Geostrophic turbulence. *J Atmos Sci*, **28**, 1087–1095.

Charney, J.G. and Eliassen, A., 1949: A numerical method for predicting the perturbations on the middle latitude westerlies. *Tellus*, **1**, No. 2, 38–54.

Craig, R.A., 1945: A solution of the nonlinear vorticity equation for atmospheric motion. *J Meteorol*, **2**, 175–178.

Derome, J., 1984: On quasi-geostrophic, finite amplitude disturbances forced by topography and diabatic heating. *Tellus*, **36A**, 313–319.

Eady, E.T., 1949: Long waves and cyclone waves. *Tellus*, **1**, No. 3, 33–52.

Ertel, H., 1943: Uber stationäre oszillatorische Luftströmungen auf der rotierenden Erde. *Meteorol Z*, **60**, 332–334.

Ferrel, W., 1856: An essay on the winds and the currents of the oceans. Reprinted (1882) in *Popular essays on the movements of the atmosphere*, Prof. papers Signal Service (Washington), **12**, 7–19.

Green, J.S.A., 1970: Transfer properties of the large-scale eddies and the general circulation of the atmosphere. *Q J R Meteorol Soc*, **96**, 157–185.

Haines, K. and Marshall, J., 1987: Eddy-forced coherent structures as a prototype of atmospheric blocking. *Q J R Meteorol Soc*, **113**, 681–704.

Held, I.M., Panetta, R.L. and Pierrehumbert, R.T., 1985: Stationary external Rossby waves in vertical shear. *J Atmos Sci*, **42**, 865–883.

Hide, R., 1988: Studies of geostrophic turbulence, chaos and other non-linear phenomena in rotating fluids: the role of combined laboratory and numerical experiments. *Meteorol Mag*, **117**, 33–34.

Hoskins, B.J., 1983: Dynamical processes in the atmosphere and the use of models. *Q J R Meteorol Soc*, **109**, 1–21.

Hoskins, B.J., McIntyre, M.E. and Robertson, A.W., 1985: On the use and significance of isentropic potential vorticity maps. *Q J R Meteorol Soc*, **111**, 877–946.

Hou, A.Y. and Farrell, B.F., 1986: Excitation of nearly steady finite-amplitude barotropic waves. *J Atmos Sci*, **43**, 720–728.

Kuo, H.L., 1959: Finite-amplitude three-dimensional harmonic waves on the spherical earth. *J Meteorol*, **16**, 524–534.

Lorenz, E.N., 1967: The nature and theory of the general circulation of the atmosphere. Geneva, WMO No. 218, TP. 115.

McWilliams, J.C., 1980: An application of equivalent modons to atmospheric blocking. *Dyn Atmos Oceans*, **5**, 43–66.

Marshall, J.C. and Nurser, G., 1986: Steady, free circulation in a stratified quasi-geostrophic ocean. *J Phys Oceanogr*, **16**, 1799–1813.

Marshall, J.C. and So, D.W.K., (1989): Thermal equilibration of planetary waves. Submitted to *J Atmos Sci.*

Mitchell, H.L. and Derome, J., 1983: Blocking-like solutions of the potential vorticity equation: their stability at equilibrium and growth at resonance. *J Atmos Sci*, **40**, 2522–2536.

Neamtan, S.M., 1946: The motion of harmonic waves in the atmosphere. *J Meteorol*, **3**, 53–56.

Niiler, P.P., 1966: On the theory of wind-driven ocean circulation. *Deep Sea Res*, **13**, 597–606.

Pearce, R.P., 1985: The global atmospheric circulation and weather forecasting. *In* Recent advances in meteorology and physical oceanography. Royal Meteorological Society.

Pierrehumbert, R.T. and Malguzzi, P., 1984: Forced coherent structures and local multiple equilibria in a barotropic atmosphere. *J Atmos Sci*, **41**, 246–257.
Read, P.L., Rhines, P.B. and White, A.A., 1986: Geostrophic scatter diagrams and potential vorticity dynamics. *J Atmos Sci*, **43**, 3226–3240.
Rhines, P.B. and Young, W.R., 1982: Homogenization of potential vorticity in planetary gyres. *J Fluid Mech*, **122**, 347–367.
Shutts, G.J., 1983: The propagation of eddies in diffluent jet-streams: eddy vorticity forcing of 'blocking' flow fields. *Q J R Meteorol Soc*, **109**, 737–761.
—, 1987a: Persistent anomalous circulation and blocking. *Meteorol Mag*, **116**, 116–124.
—, 1987b: Some comments on the concept of thermal forcing. *Q J R Meteorol Soc*, **113**, 1387–1394.
Smagorinsky, J., 1953: The dynamical influence of large-scale heat sources and sinks on the quasi-stationary mean motions of the atmosphere. *Q J R Meteorol Soc*, **79**, 342–366.
Stern, M.E., 1975: Minimal properties of planetary eddies. *J Mar Res*, **33**, 1–13.
Tribbia, J.J., 1984: Modons in spherical geometry. *Geophys Astrophys Fluid Dyn*, **30**, 131–168.
Verkley, W.T.M., 1984: The construction of barotropic modons on a sphere. *J Atmos Sci*, **41**, 2492–2504.
—, 1987: Stationary barotropic modons in westerly background flows. *J Atmos Sci*, **44**, 2383–2398.
—, 1988: On atmospheric blocking and the theory of modons. (Ph D thesis, University of Amsterdam.)
White, A.A., 1986: Finite amplitude, steady Rossby waves and mean flows: analytical illustrations of the Charney-Drazin non-acceleration theorem. *Q J R Meteorol Soc*, **112**, 749–773.
Young, W.R. 1987: Selective decay of enstrophy and the excitation of barotropic waves in a channel. *J Atmos Sci*, **44**, 2804–2812.
Zhang, X., Zeng, Q. and Bao, N. 1986: Nonlinear baroclinic Haurwitz waves. *Adv Atmos Sci*, **3**, 330–340.

551.466.3:551.501.7

Remotely sensed data for wave forecasting

R.A. Stratton
Meteorological Office, Bracknell

Summary

Measurements of wave height and wind speed will be available, after the launch, from the altimeter on ERS-1. The effects of assimilating such data in a global wave model have been investigated using altimeter measurements from SEASAT and GEOSAT. The assimilation improves agreement between the model and the altimeter wave-heights, and it is still evident in a 5-day forecast. These results provide encouragement for the future use of altimeter data.

1. Introduction

ERS-1, the first European Remote Sensing satellite (Duchossois 1983), is scheduled to be launched in 1990. The satellite will carry a radar altimeter, and a wind scatterometer. The instrument of use to wave modellers and forecasters is the altimeter, which is capable of measuring surface wind speed and significant wave height, every second, over a footprint of several square kilometres directly below the satellite. The wind scatterometer also measures surface wind speed and direction over the sea surface, to one side of the satellite track. The data from the altimeter and the wind scatterometer are expected to be available to users within 3 hours of measurement, making it possible to use such data in operational weather and wave forecasting. In this paper the assessment of radar altimeter data only is discussed

At present the Meteorological Office runs two operational wave models: a global version, and a European version covering the North Sea, the Baltic and the Mediterranean. Both models are driven by wind fields from the lowest level of the corresponding numerical weather prediction (NWP) model (Bell and Dickinson 1987).

The Meteorological Office's wave models specify the energy density, $E(f,\theta)$, at each model grid-point where f is the frequency and θ the direction. Wave energy is related to the total surface height variance. The basic physics used for wave growth and dissipation is an improved version of that described by Golding (1983). An extra term has been added to improve the wave model spectrum in situations where the model wind direction turns quickly. A correction term has been added to the advection scheme to ensure that energy moves on great circles.

Actual wave observations are not used to initialize either of the wave models in the present operational suite. Instead the wave forecast is preceded by a wave hindcast to provide an initial wave field. The wave hindcast is a 12-hour wave model run using winds from the NWP assimilation. The hindcast run starts from the wave field at the end of the preceding hindcast. This provides a better initial wave field for the next wave forecast than a wave field obtained from the previous forecast.

To fully initialize a global wave model requires full wave spectral measurements and wind measurements

distributed evenly over the world's oceans. A wave spectrum can consist of either a full two-dimensional spectrum of the energy density in each frequency and direction, or a one-dimensional spectrum where only the energy in each frequency is known. If the full wave spectral information is not available, integrated parameters, e.g. wave height and wave period, could be used instead. The problems with using integrated data are mentioned in section 2.

At present wave spectral information is scarce and not generally available. Some buoys, and new instruments deployed on satellites and aircraft, can measure spectral information, but it is not always easy to interpret the satellite return signals in such a way as to generate the original full two-dimensional wave spectrum in an unambiguous fashion.

Up to now the only sources of wave data have been buoys, ocean weather ships, oil platforms and ships of passage. The ship observations (while the most numerous) are normally visual estimates, and therefore are not regarded as accurate and reliable enough for use in verification or initialization of wave model forecasts. Fig. 1 shows the location of the buoys, ocean weather ships and oil platforms reporting regularly (usually every hour) wave height, wind speed and wave period. The oil platforms are located in the North Sea. Apart from three weather ships across the Atlantic, the rest of the stations are located within a few hundred kilometres of the coast. There is virtually no data in the southern hemisphere. The lack of data and the concentration of what there is along the coasts do not provide a good coverage of the world's oceans. Data assimilation into the global wave model using the present data would not be worthwhile.

In recent years several new techniques for measuring waves have been developed. These have led to the use of high frequency radar to measure wave heights near to the coast, and radar altimeters to measure wave height and surface wind speed over the open ocean. In 1978 the satellite SEASAT was launched with a radar altimeter, wind scatterometer and synthetic aperture radar on board. The satellite operated for 3 months before failing, providing a large amount of data, the full potential of which has only recently been exploited for wave modelling. In 1985, GEOSAT, a USA naval satellite with a radar altimeter was launched, and is still functioning. Fig. 2 shows the satellite ground track for GEOSAT for a period of 24 hours. The coverage of the oceans is far better than shown in Fig. 1 and makes wave data assimilation appear worth investigating ready for

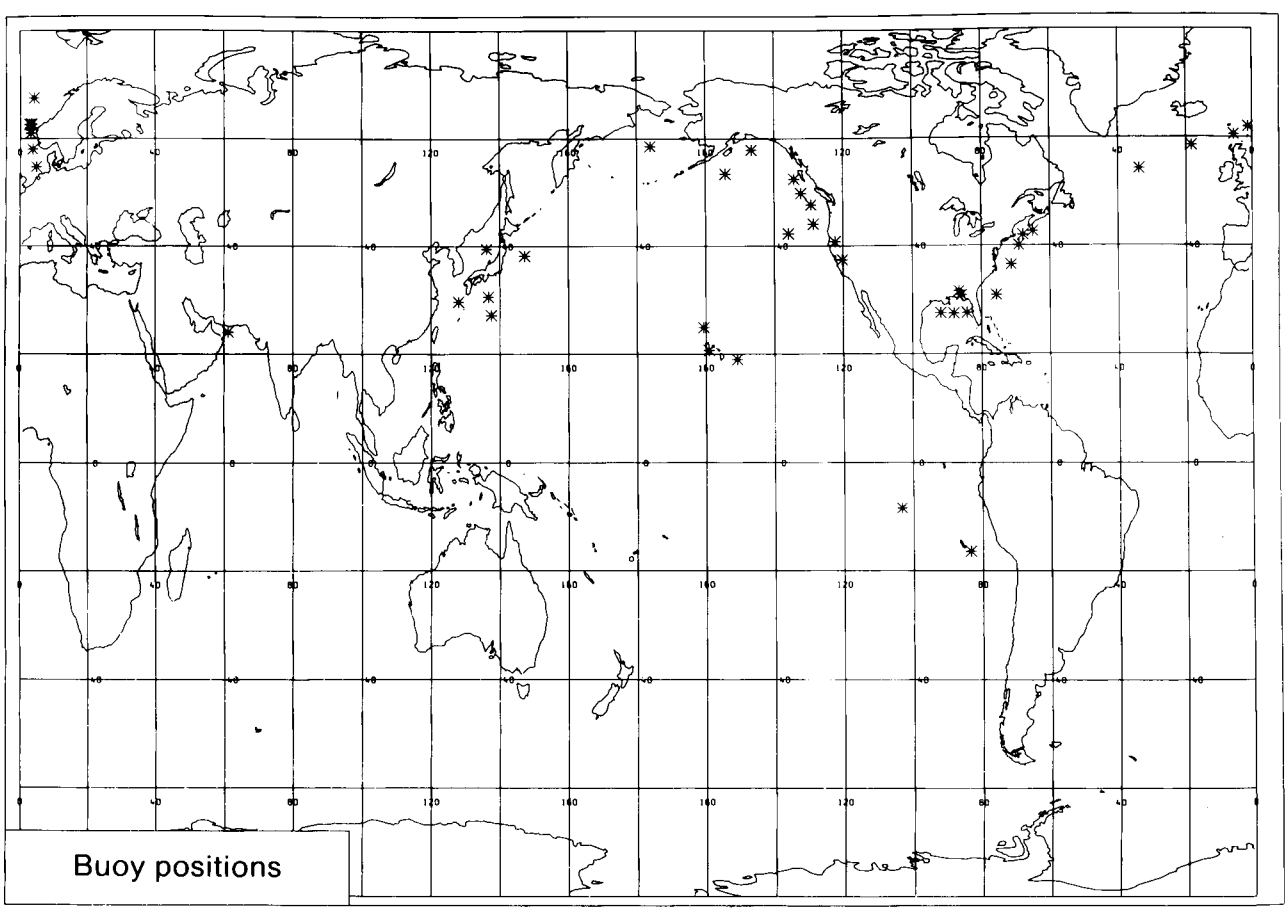

Figure 1. The location of buoys, oil platforms and ocean weather ships reporting wave heights used regularly in operational verification of the Meteorological Office's global wave model. Each station is plotted as an asterisk.

the launch of ERS-1. ERS-1 is expected to have similar global coverage in a 24-hour period to that shown in Fig. 2.

To develop an assimilation scheme for the wave data from ERS-1, it is necessary to use satellite data from the past. The data from GEOSAT has recently become available and has been used in addition to SEASAT data to develop a wave data assimilation scheme for the Meteorological Office's global wave model. The results of wave data assimilation using SEASAT and GEOSAT data are described in section 3.

2. Using remotely sensed data in a wave model

The most useful form of wave measurements for assimilation would be two-dimensional wave spectral data, but this is not available, so integrated parameters such as significant wave height must be used instead. Significant wave height, H_S, is given by

$$H_S = 4\sqrt{E_{TOT}}$$

where E_{TOT}, the wave energy as calculated by the model, is in units of m^2 and

$$E_{TOT} = \int E(f,\theta)\, d\theta\, df$$

the integral of the energy density (in units of m^2 s rad^{-1}) over direction, θ, and frequency, f.

It is not a simple matter to turn a measurement of H_S into an energy density spectrum which can be used to adjust the model value. A scheme to retrieve an energy density spectrum from a wave height measurement, making use of a co-located wind speed measurement, has been described by Thomas (1988). A modified version of this scheme has been applied to retrieving an energy spectrum for assimilation into the global wave model (Francis and Stratton 1990). The assimilation scheme used is a successive correction scheme, i.e. it makes use of the observations at their datum time, and spreads the influence of the observation over neighbouring grid-points. Observations are assimilated every hour into the global wave model.

The accuracy and spatial representativeness of an observation need to be considered in order to make good use of any data in an assimilation scheme. The altimeter algorithms determine the wave height and wind speed by measuring the return signal received by the satellite when it sends out a pulse of microwave energy down to the ocean below. The pulse emitted by the radar altimeter has a rectangular shape which is distorted by the uneven sea surface. Energy reflected by the wave-peaks returns to the altimeter sooner than

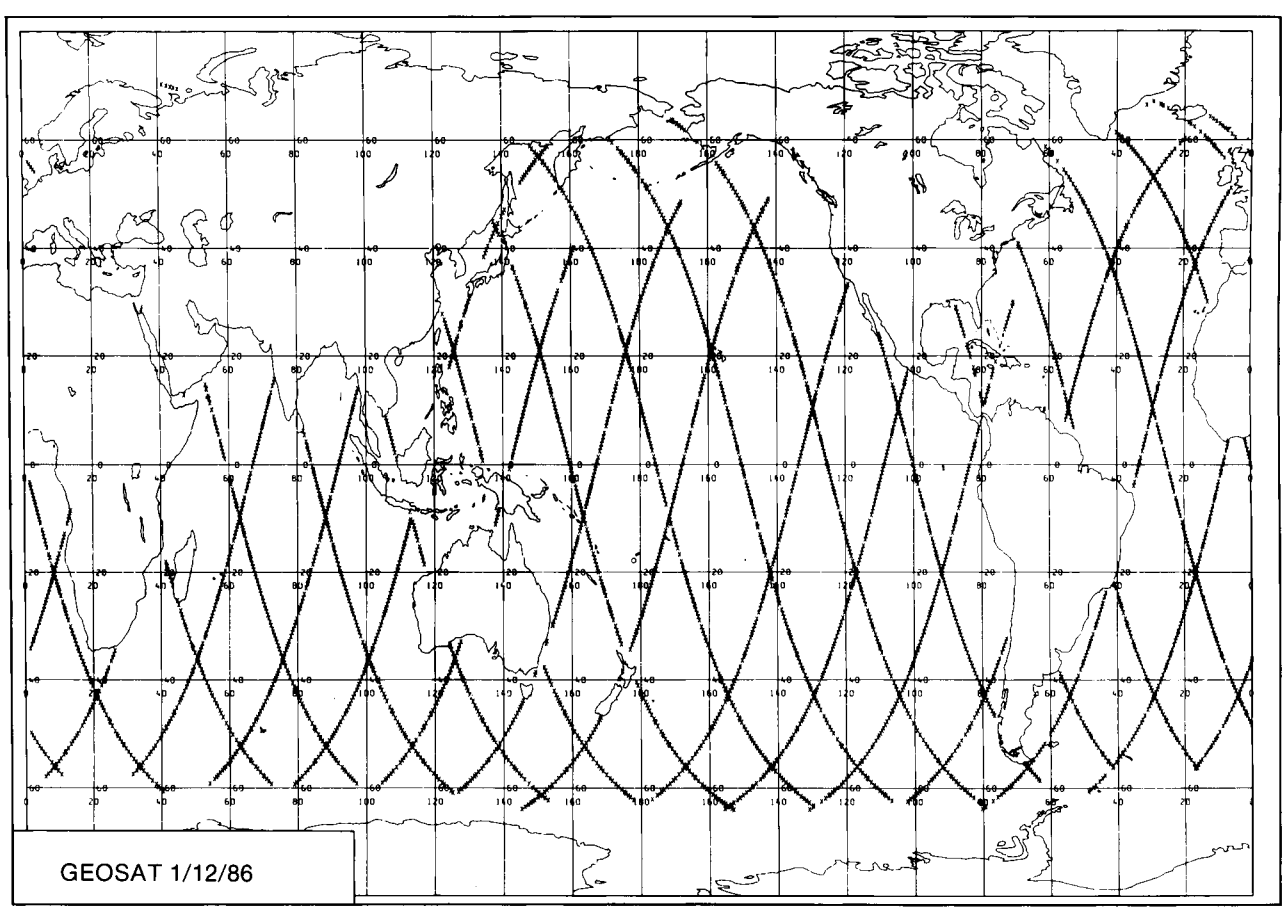

Figure 2. The coverage of quality controlled and averaged GEOSAT altimeter measurements for 24 hours (1 December 1986).

energy reflected from the troughs, leading to a sloped return pulse. The algorithm for wave height uses the slope of the return pulse to calculate the wave height. The wave height algorithm has been compared with buoy measurements up to wave heights of 6 metres, with good agreement (Fedor and Brown 1982, for SEASAT data, and Dobson *et al.* 1987 for GEOSAT data). The altimeter accuracy is usually specified as ±10% or ±0.5 m whichever is the larger for wave height measurements. Most buoys measure to ±0.5 m.

The wind speed algorithm depends on the backscatter cross-section. There are several different algorithms in existence but they are inaccurate at high wind speeds where the incident microwave energy is scattered more widely by the rough sea surface; hence the energy scattered back to the altimeter is very small, and small differences in the backscatter can produce large differences in the retrieved wind speed. The altimeter accuracy is specified as ±2 m s^{-1} for wind speeds up to 18 m s^{-1}. Buoys usually measure to ±1 m s^{-1} or ±10%.

The altimeters operated so far have produced measurements at intervals of about 1 second in time and between 5 and 10 km in distance. The resolution of the present global wave model is approximately 150 kilometres. The SEASAT and GEOSAT altimeter measurements are averaged over 20 seconds to create observations of spatial resolution approximately equal to that of the wave model. As part of the averaging process the altimeter data are quality controlled to remove measurements over ice, close to coasts or significantly different from adjacent values.

3. Wave data assimilation experiments

Until the mid 1980s very little work had been done on developing assimilation schemes for wave models. Since then the ideas put forward by Thomas (1988) have been applied in different ways by several other groups to data assimilation using SEASAT altimeter data (Janssen *et al.* 1989, Esteva 1988 and Hasselmann *et al.* 1988).

So far two different sources of satellite altimeter data have been used in wave data assimilation experiments at the Meteorological Office. The first experiments used data from SEASAT for a period of 6 days starting on 15 September 1978. The second set of experiments used GEOSAT data for 31 days in 1986 starting on 11 November.

3.1 SEASAT data assimilation

A detailed account of the SEASAT assimilation experiments is given in Francis and Stratton (1990) and will not be repeated here. The main objective of the SEASAT work was to show that altimeter data could be successfully assimilated into a wave model, and that improvement of the wave field and the following forecast would result. This was achieved by first running the global wave model for the 6 days in September 1978, without assimilation, to produce a control run. The resulting wave heights were then compared with the averaged altimeter values. The run was then repeated, assimilating wave data for 24 hours, followed by a further 5 days running without assimilation (experiment 1), in order to assess the impact of the added data. Finally the assimilation was continued for the full 6 days (experiment 2), to see if the wave field required a 'warm up' period to adjust fully to the assimilated data.

Fig. 3 shows the main results of the three runs in the form of a time-series plot of daily mean and root-mean-square differences, for the altimeter minus the model wave heights. The 24-hour assimilation (experiment 1) reduced the mean wave height difference, for the whole globe, between the altimeter data and the wave model from 0.8 m to 0.3 m. The difference relaxed back towards 0.8 m over the following 5 days. This implies that corrections to the initial wave field may have an impact on the following wave forecast even at the end of 5 days. Continuous assimilation (experiment 2) resulted in the wave heights moving closer to the altimeter values. By 19 September the bias was almost zero. Continuous assimilation did not result in a significant further reduction of the root-mean-square difference after the initial fall on 15 September. This suggests that the root-mean-square difference has reached a lower limit imposed by the errors contributed by the model and its driving winds.

Comparison of the model wave heights from the control run, with the altimeter values for the whole globe, gave a mean difference of −0.8 m (model minus altimeter value), and a standard deviation of 1.0 m. The corresponding wind speed differences were a mean scalar difference of −0.4 m s^{-1} and a standard deviation of 3.0 m s^{-1}. This is consistent with the suggestion that the underestimation in wave height is caused by the model winds being too low. The SEASAT altimeter wave heights used in the experiments were calculated using an algorithm which has been shown (Fedor and Brown 1982) to overestimate wave height by 0.5 m for wave heights above 2 m. Hence the altimeter wave heights may be too high, so that the underestimation of the model waves relative to the altimeter values may be too large.

3.2 GEOSAT data assimilation

The GEOSAT data provided an opportunity to investigate the results of assimilating altimeter data into a wave model during the northern hemisphere winter. In 1986 there were far more buoy reports available than in 1978 and so it was possible to use the buoy data as an independent means of checking the results of the assimilation.

The global wave model was run for 31 days starting on 11 November 1986 to provide a control run, and the resulting wave heights were compared with the averaged altimeter wave heights for the last 27 days. The 31-day GEOSAT run was repeated, this time assimilating altimeter data into the wave model, and the results for the last 27 days were compared with those of the control

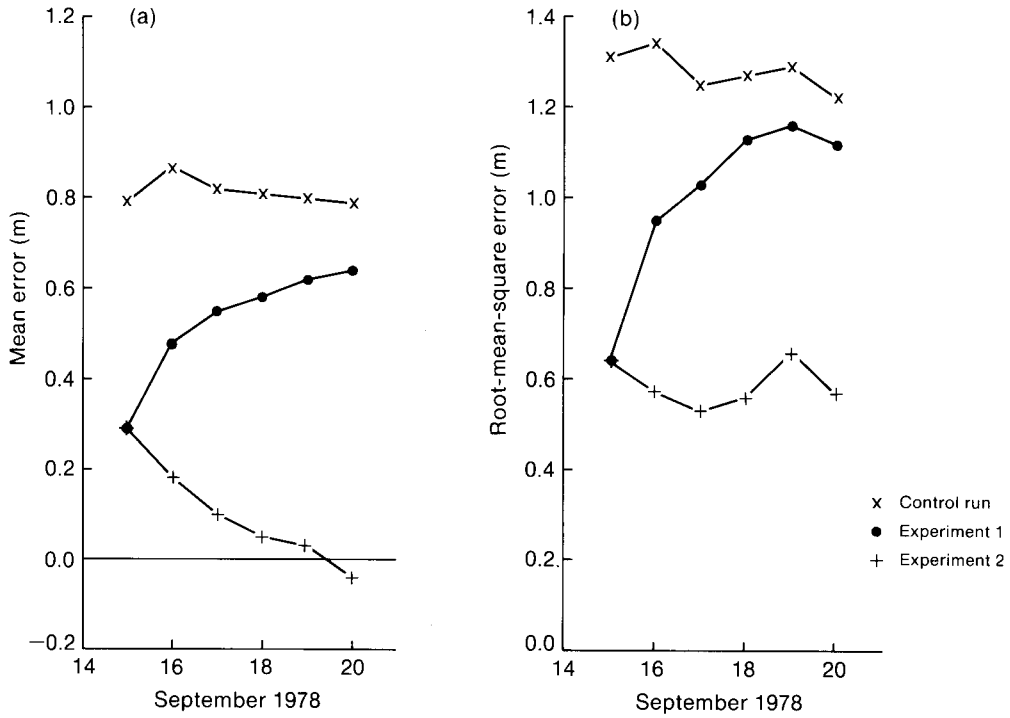

Figure 3. The SEASAT control run and experiments 1 and 2 wave height (observed–model) errors; (a) mean and (b) root-mean-square values.

run. The first 4 days were omitted from the comparison to allow the model to adjust to the assimilated data. Table I gives the results of the comparison of the model wind speeds and wave heights against the averaged altimeter values, broken down into latitude bands for both the control and assimilation runs. The model wind speeds are biased lower than the altimeter values for the whole globe with model wind speeds being higher than the measured values in the northern hemisphere between 20° and 60°N. The largest number of winds greater than 15 m s^{-1} are observed by the altimeter in this region. In the northern hemisphere the NWP analysis of deep depressions with strong surface winds is likely to be better than in the southern hemisphere because of the greater number of observations, hence the model prediction of high waves will be better in the northern hemisphere.

The wave height differences for the latitude bands show the effect of the bias in wind speeds, the model wave heights being lower than the altimeter in the south and higher in the north. In the assimilation run, the overall bias is modified so that model values are higher than altimeter values in all areas. The assimilation of wave data reduces the spread of differences, as found in the SEASAT work, but this time as the GEOSAT retrieval algorithm gives unbiased wave heights, the mean difference is not substantially changed. In fact the mean difference changes from an underestimation for the low waves (0–3 m) to an overestimation. This may indicate that the wave model does not dissipate swell

Table I. Wave height and wind speed difference statistics for the GEOSAT control and assimilation runs 00 UTC on 15 November 1986 to 00 UTC on 12 December 1986. Differences are model minus altimeter average.

Latitude range (°)	Wind speed (m s^{-1})			Wave height (m)				
				Control			Assimilation	
	Number	Mean	s.d.	Number	Mean	s.d.	Mean	s.d.
40–60 N	6 745	1.1	3.7	7 210	0.6	1.0	0.2	0.6
20–40 N	11 399	0.5	2.5	11 415	0.2	0.6	0.2	0.4
0–20 N	15 639	−0.3	2.5	15 663	0.1	0.6	0.2	0.4
20–0 S	15 902	−0.5	2.0	15 916	−0.1	0.4	0.2	0.3
40–20 S	19 282	−0.5	2.3	19 297	−0.3	0.6	0.1	0.3
60–40 S	25 969	−0.3	3.0	26 002	−0.4	0.9	0.1	0.5
All	98 551	−0.2	2.7	99 321	−0.1	0.8	0.1	0.4

energy quickly enough, or that the assimilation process is spreading energy into the wrong directions.

The results from latitudes 20°–60°N have been studied further by comparing the differences between the model and altimeter with those found between the model and buoy or ocean weather ship reports. Table II gives the wind speed difference statistics broken down into several wind speed ranges. At low wind speeds both the altimeter and the buoy values are lower than the model. Whereas buoys measure wind speeds at heights between 6 m and 10 m above mean sea level, ocean weather ships measure values at 19.5 m, and the altimeter algorithm is valid for winds at 19.5 m. Since model wind speeds are at a nominal height of 20 m, it is not surprising that the buoy values are lower than those of the model. Comparison of the model wind speeds with the altimeter values shows that altimeter algorithm also underestimates the wind speeds below 15 m s^{-1}. At winds greater than 15 m s^{-1} the wave heights can exceed 5 m. Measurements of high wind speeds by buoys with anemometer heights of only 6 m may be affected by such high waves. At higher wind speeds, as mentioned in section 2, the algorithm is no longer reliable. The scatter in the differences increases with wind speed for both buoys and altimeter measurements. These results show that altimeter wind speeds must be used with some caution, particularly at high wind speeds. However, in view of their co-location with the altimeter wave-height measurements, the wind speeds remain an acceptable source of data for the assimilation scheme.

The wave-height difference statistics are given in Table III (model minus altimeter) and Table IV (model

Table II. Wind speed difference statistics for the GEOSAT control run 00 UTC on 15 November 1986 to 00 UTC on 12 December 1986. Values given are for model minus altimeter and model minus buoy/weather ship for latitudes 20°–60°N.

Wind-speed range (m s^{-1})	Model–altimeter (m s^{-1})			Model–buoy/ship (m s^{-1})		
	Number	Mean	s.d.	Number	Mean	s.d.
0–10	13 198	0.5	2.5	6230	0.8	2.4
10–15	4 414	1.6	3.6	2115	1.0	3.0
> 15	532	−0.7	4.8	1053	−0.1	3.5
All	18 144	0.7	3.0	9398	0.7	2.7

Table III. Wave height difference statistics for GEOSAT data 00 UTC on 15 November 1986 to 00 UTC on 12 December 1986 Values are for model minus altimeter. Latitude band 20°–60°N.

Wave-height range (m)	Control (m)			Assimilation (m)	
	Number	Mean	s.d.	Mean	s.d.
0–3	11 679	0.3	0.6	0.2	0.4
3–6	6 069	0.5	1.0	0.2	0.6
> 6	877	0.8	1.3	0.1	0.8
All	18 625	0.4	0.8	0.2	0.5

Table IV. Wave height difference statistics for buoys and weather ships, 00 UTC on 15 November 1986 to 00 UTC on 12 December 1986. Values are for model minus observation.

Wave-height range (m)	Control (m)			Assimilation (m)	
	Number	Mean	s.d.	Mean	s.d.
0–3	5163	0.2	0.7	0.2	0.6
3–6	2997	0.2	1.0	0.1	0.9
> 6	1183	0.4	1.6	−0.1	1.5
All	9343	0.2	1.0	0.1	0.9

minus buoy/ocean weather ship). The results show that the model overestimates wave heights when compared with both altimeter and buoy values. This overestimation is consistent with the overestimation of wind speeds found in Table II. The differences increase with wave height. The assimilation process, as might be expected, reduces the difference between the altimeter and model values, to 0.2 m for 0–6 m waves and to 0.1 m for waves greater than 6 m. The assimilation scheme has a greater impact on the higher waves which are mainly due to the local wind. The buoy statistics are also improved particularly at high wave heights (> 6 m), changing the model bias from an overprediction to underprediction relative to the buoy/ship measurements. This may indicate a difference in the calibration of the altimeter and the buoy/ship measurements. The process whereby the assimilation scheme adjusts the model at the buoy locations is indirect, as satellite overpasses are relatively few. The improvement in agreement between the model and the buoy values comes mainly from energy propagated outwards from corrections made to the model along the satellite track.

Figs 4(a) and 4(b) show time-series of wind speeds and wave heights for 5 days in December at the ocean weather station Lima. The wind time-series, Fig. 4(a), shows an error in timing between the model and the

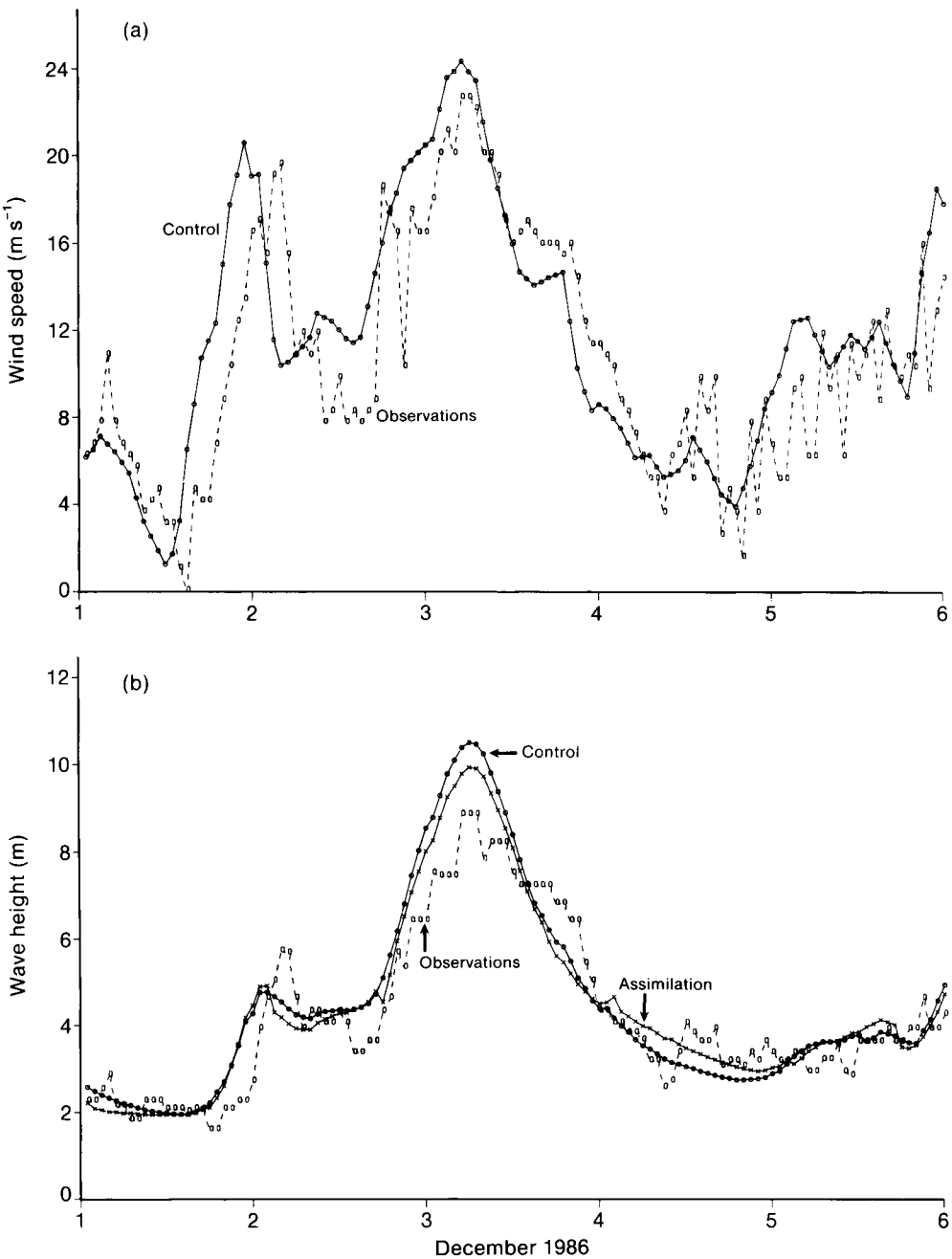

Figure 4. Time-series for ocean weather ship Lima (57° N, 20° W) for 5 days in December 1986 for (a) wind speed and (b) wave height. All values are plotted hourly.

observed wind peak on 2 December whereas the peak on the 3rd is well represented. This is also seen in the wave-height plot (Fig. 4(b)). The control wave-height for the second peak is of the order of 1.5 m higher than that estimated at the ocean weather ship. An overpass of the satellite assimilated about 18 UTC on 2 December reduces the model peak on the 3rd by 0.5 m. Further assimilation on 4 December prevents the wave height from dropping below the reported value. Figs 5 and 6 show wave isopleths for 06 UTC on 3 December for the control and assimilation runs respectively. The wave heights of the storm areas are reduced in the assimilation run, for example in the area around 55° N, 20° W where the peak is reduced from 10.7 m to 10 m. The maximum wave height near to 35° N, 70° W is also reduced from 6 m to 5 m.

4. Conclusions

The SEASAT study demonstrates that satellite measurements of co-located wave heights and wind speeds can be successfully used in a global wave model assimilation scheme. The wave height can be adjusted by the assimilation process to fit the altimeter measurements, improving the agreement between the following hindcast and the altimeter. The results of the assimilation persist for at least 5 days and may improve the operational global wave model 5-day forecasts. The largest improvements are found in the southern hemisphere where the driving winds are not so well analysed due to the lack of observations in the atmospheric assimilation.

After the launch of the ERS-1 scatterometer, wind data will be used in the atmospheric assimilation scheme and therefore the quality of the surface winds should improve in the southern hemisphere.

The GEOSAT study has shown that the global wave model agrees well with the altimeter measurements of wave height before assimilation. Assimilation of the altimeter data reduces the differences between the altimeter and the wave model, but individual time-series show that the altimeter corrections do not always agree with the buoy or ship observations. This study has also shown that in a northern hemisphere winter month the use of altimeter data in assimilation does improve the overall agreement between the model and independent reports from buoys or ocean weather ships.

So far no work has been done on assimilating data into a shallow-water wave model like the Meteorological Office's European wave model. Before assimilating data into such a model it will be necessary to develop a

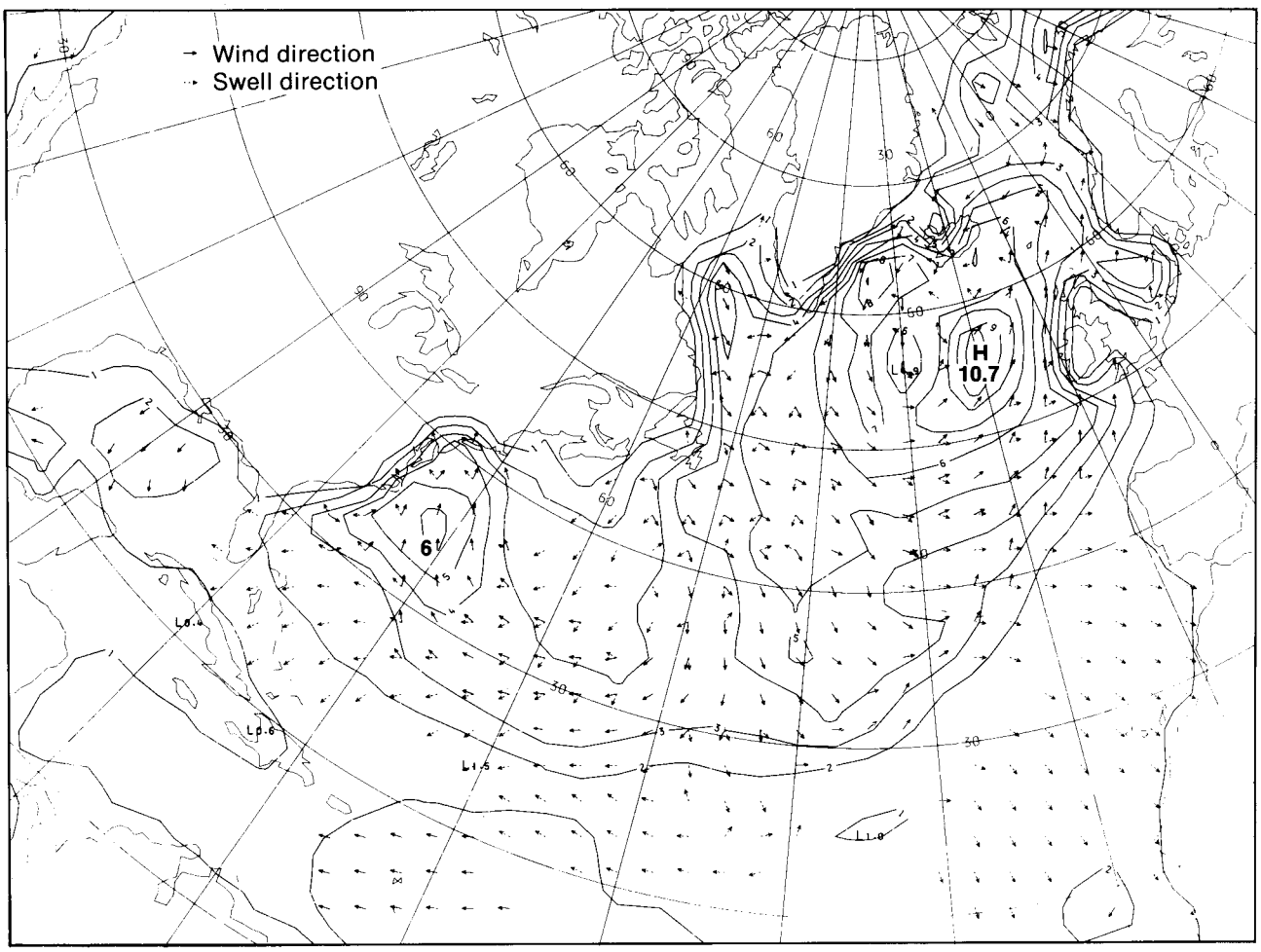

Figure 5. Wave height (m) isopleth chart for the North Atlantic 06 UTC on 3 December 1986 from the control run.

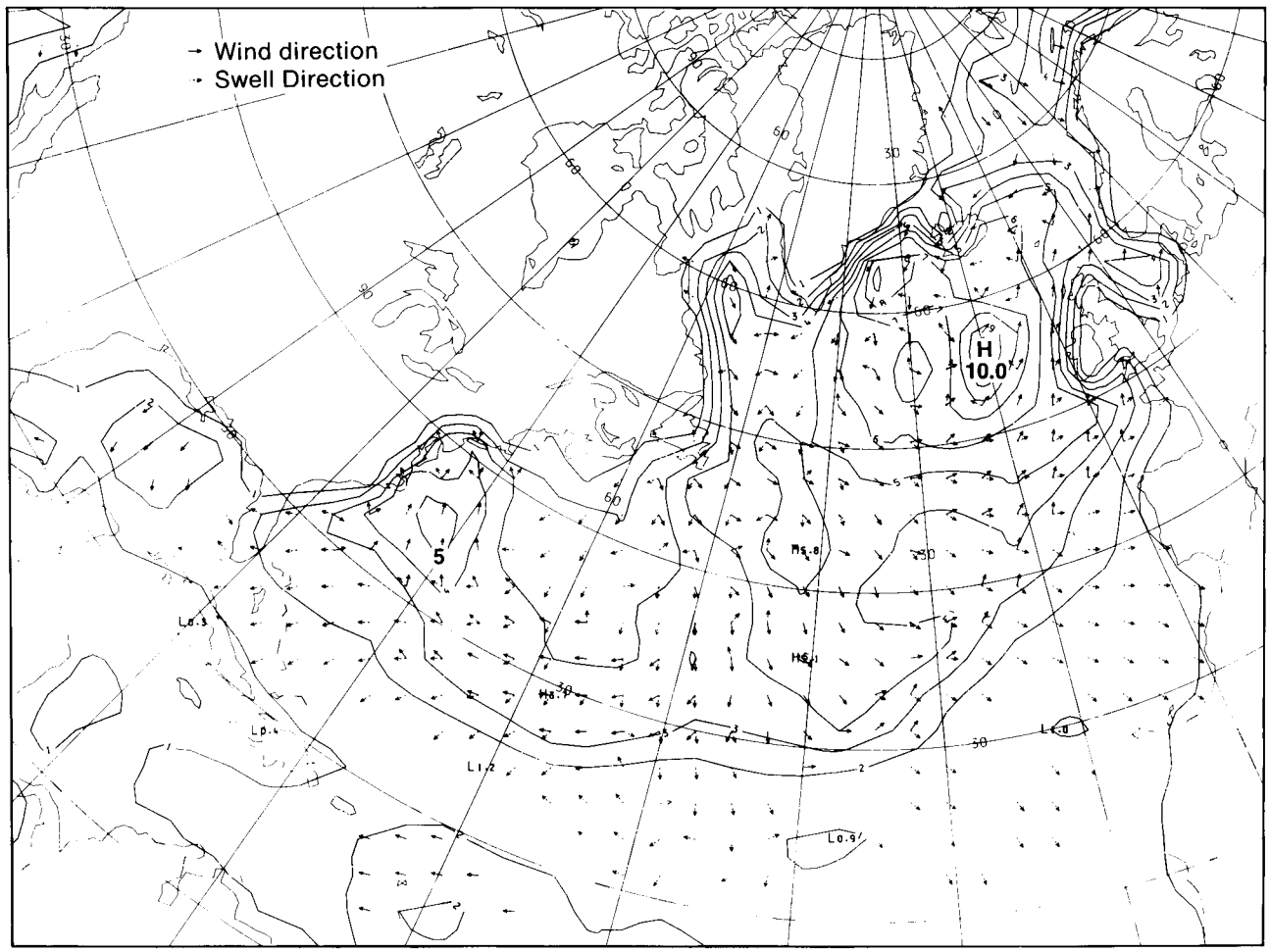

Figure 6. As Fig. 5 but from a run assimilating GEOSAT data.

method to spread the influence of an observation over an area of sea with varying depth.

If spectral wave data becomes available in the future it should be relatively simple to extend the existing wave assimilation scheme. Two-dimensional wave spectra can be used directly in the assimilation process. These developments are possibilities for the future, in the meantime we may look forward to making use of the wind and wave data from ERS-1.

Acknowledgements

The assistance of K. Rider throughout this work is gratefully acknowledged.

References

Bell, R.S. and Dickinson, A., 1987: The Meteorological Office operational numerical weather prediction system. *Sci Pap, Meteorol Off*, No. 41.

Dobson, E., Monaldo, F., Goldhirsch, J. and Wilkerson, J., 1987: Validation of GEOSAT altimeter derived wind speeds and significant wave heights using buoy data. Baltimore, Maryland, Johns Hopkins University, Applied Physics Laboratory, *Tech Dig*, **8**, No. 2, 222–234.

Duchossois, G., 1983: The first European remote sensing satellite (ERS-1): Overall description, potential applications and users. European Space Agency (ESA) SP-205, 25–36.

Esteva, D.C., 1988: Evaluation of preliminary experiments assimilating SEASAT significant wave heights into a spectral wave model. *J Geophys Res*, **93**, 14099–14105.

Fedor, L.S. and Brown, G.S., 1982: Wave height and wind speed measurements from the SEASAT radar altimeter. *J Geophys Res*, **87**, 3254–3260.

Francis, P.E. and Stratton, R.A., (1990): Some experiments to investigate the assimilation of SEASAT altimeter wave height data into a global wave model. (Submitted to *Q J R Meteorol Soc.*)

Golding, B., 1983: A wave prediction system for real-time sea state forecasting. *Q J R Meteorol Soc*, **109**, 393–416.

Hasselmann, K., Hasselmann, S., Bauer, E., Bruning, C., Lehner, S., Graber, H. and Lionello, P., 1988: Development of a satellite SAR image spectra and altimeter wave height data assimilation system for ERS-1. Max Planck Institute for Meteorology, report No. 19, European Space Agency contract report, contract No. 6875/87 HGE I(SC).

Janssen, P.A.E.M., Lionello, P., Reistad, M. and Hollingsworth, A., 1989: Hindcast and data assimilation studies with the WAM model during the SEASAT period. *J Geophys Res*, **94**, 973–993.

Thomas, J.P., 1988: Retrieval of energy spectra from measured data for assimilation into a wave model. *Q J R Meteorol Soc*, **114**, 781–800.

Award

The Rank Prize Fund Award for Opto-electronics, 1989

In 1972, in accordance with the wishes of the late Lord Rank, a fund was set up for prizes to be awarded to researchers making significant advances in opto-electronics.

Prizes from this fund have been awarded to a group of workers responsible for the design and use of the Pressure Modulator Radiometer (PMR) for investigating the temperature of atmospheres and the concentration of gaseous components. The group consists of Drs F.W. Taylor, G.D. Peskett and C.D. Rodgers of the Department of Atmospheric, Oceanic and Planetary Physics, Clarendon Laboratory, Oxford and Dr J.T. Houghton, formerly at Oxford, but now Director-General of the Meteorological Office.

The PMR is a device which enables the outgoing radiation (often very weak) from different gases in a planetary atmosphere, and from different levels, to be measured. Radiation which is easily absorbed can only escape from the upper layers of an emitting gas, while radiation which is only slightly absorbed can travel upwards from lower layers. The radiation observed depends upon the temperature and concentration profiles of the gas — if one is known then the other can be estimated from the observations. The absorption depends upon the precise wavelength of observation, so in principle a few narrow spectral bands at carefully selected wavelengths could be used to measure radiation from a chosen range of layers of an atmosphere. The penalty is that the radiation in individual narrow wavebands is very small.

This problem can be overcome by observing the strength of the upwelling radiation alternately through a cell containing the gas of interest and through an empty one a combination which acts like a filter with numerous spectral slits. The general level of the atmosphere from which the radiation is emitted is determined by the cell gas pressure. The disadvantage is the difficulty of maintaining stable optical balance of the two cells. In the PMR, only one cell is used, the gas pressure being modulated sinusoidally by a piston in a connecting cylinder and the amplitude of the difference signal at that frequency is related to the radiation from levels above those observed with an unmodulated cell. A further benefit is that the piston frequency can be made to indicate the cell gas pressure, allowing calibration remotely. An adaptation of the PMR utilizing the 'Stirling cycle' is also used to cool the radiation detectors to low temperatures to increase their sensitivity.

PMRs designed and built at the Clarendon Laboratory and by the Meteorological Office have been flown on several earth satellites. Observations of CO_2, with its constant known mixing ratio, enable the temperature profile to be deduced. Observations of the radiation from other trace gases (the oxides of nitrogen, for instance) can then be used to deduce their concentrations. A PMR was also flown on the Pioneer Venus satellite to observe the temperature structure of the atmosphere of Venus from observations of CO_2 radiation.

The prize-giving took place at the Royal Society's meeting rooms on 26 September 1989. After a welcoming address by Sir John Davis, CVO, who is the chairman of the Trustees of the Rank Prize Funds, the awards were made by Sir George Porter (President of the Royal Society). Dr Taylor responded on behalf of the four prize winners.

On the same occasion, Dr J.L. Monteith, well known for his work on meteorological aspects of plant physiology (especially evapotranspiration), was awarded one of the Rank prizes for Nutrition, for his elucidation of the physical principles determining crop growth.

The photograph shows from left to right — Dr C.D. Rodgers, Sir George Porter, Dr F.W. Taylor, Sir John Davis, Dr J.T. Houghton and Dr G.D. Peskett.

Workshop report

Workshop on Numerical Products from Bracknell, Meteorological Office College, Shinfield Park, Reading 26–28 June 1989

A Workshop on Numerical Products from Bracknell was held at the Meteorological Office College, Shinfield Park from 26 to 28 June 1989 and was attended by some 44 delegates from 32 countries, including many forecasters and numerical modellers. The principal aim of the workshop was to describe and illustrate the range of specialized products that are derived from the Meteorological Office operational numerical weather prediction global and regional models for use by the forecasters, which could have direct application and uses in other Meteorological Services. Presentations were made to the workshop by Meteorological Office staff mostly from the Central Forecasting Office (CFO), and the Forecasting Products and Forecasting Research Branches. A brochure was prepared with the help of the Graphics Office and Editing Section containing abstracts of the presentations along with illustrations of most of the specialized products available.

The workshop was chaired jointly by Dr P. Ryder, Deputy Director (Forecasting), and Mr R. Morris, Assistant Director (Central Forecasting) who, as head of the Bracknell Regional Specialized Meteorological Centre (RSMC) for WMO, was also responsible for the organization of the workshop.

The workshop was formally opened by Dr J.T. Houghton, the Director-General of the Meteorological Office, who welcomed the delegates and pointed out the importance of the basic WMO philosophy of free exchange of data and products between Member States. No amount of sophisticated modelling or more powerful computer hardware can replace observations, and so all Members have their part to play in the process.

Following a wide-ranging and interesting review by A. Gadd of the history of the development of numerical weather prediction (NWP), there were two talks on data assimilation. Firstly, A. Lorenc described the system of four-dimensional data assimilation used in the current operational models, and then M. Stubbs described some of the techniques used by forecasters to add value to the NWP analysis, largely through skilful interpretation of satellite imagery. C. Hall showed some results from the process of monitoring the observations used by the NWP models; in particular it was shown how systematic errors could be identified in the data, which were then used to correct the data before processing. The first day was concluded with a talk from A. Woodroffe who described how forecasters in the CFO evaluate and interpret the NWP products in formulating their guidance to dependent forecasters and others.

On the following morning, the delegates were given a tour of the Richardson Wing of the Meteorological Office Headquarters, which contains the operational forecasting, telecommunications and computing centres. After lunch, the workshop reassembled to hear about developments in telecommunications from P. Sowden, who described new methods being devised to handle the increasing volume of data, including the use of communication channels on Meteosat for broadcast to Africa. This was followed by a talk from R. Morris, who demonstrated the capability of the global model to simulate the development of tropical storms and to predict the movement of these storms with some skill over 5 days ahead. An important part of the forecasting process was the fine tuning of the analysis by forecasters in the CFO, making use of local tropical cyclone advisories and satellite imagery. It was noted that the CFO had issued advisories twice daily to Member States in the South Pacific throughout the 1988/89 season. K. Pollard described the range of products that are derived from the NWP model output to help the forecaster with preparation of significant weather charts for civil aviation. Most of the weather elements that are required can now be derived directly from the model output, leaving the forecaster with the task of fine tuning the final product. Several airlines are now making more direct use of the forecast winds by having headwind components calculated for specific routes, for example.

P. Francis spoke about the Meteorological Office wave and storm surge models, the wave model using the NWP model predictions of surface wind to calculate the wave heights and periods, and also the spectrum of energy levels. The storm surge model is used principally to predict tidal levels around the UK continental shelf, but the model can be applied wherever coastal areas are prone to tidal flooding. Finally, M. Cullen outlined the specification of the new unified model which will become operational on the supercomputer in 1990. The new global model will have a grid length only slightly greater than the current regional model and will therefore be able to simulate smaller-scale features such as tropical cyclones more realistically than hitherto.

There were two open forums chaired by H. Lyne in which the delegates were invited to comment on products that are available to Member States. Feedback on the usefulness of the products was regarded as essential, and it was important to know whether national requirements would be satisfied by the new products being developed at Bracknell.

It was concluded that the workshop had achieved its prime objective of creating a greater awareness of the range and quality of NWP products available at Bracknell RSMC. In turn, the delegates were conscious of the importance of timely and accurate observations without which numerical modelling would be of little value.

B.K. Lloyd

Radar photographs — 8 November 1989 at 0600 and 1200 UTC

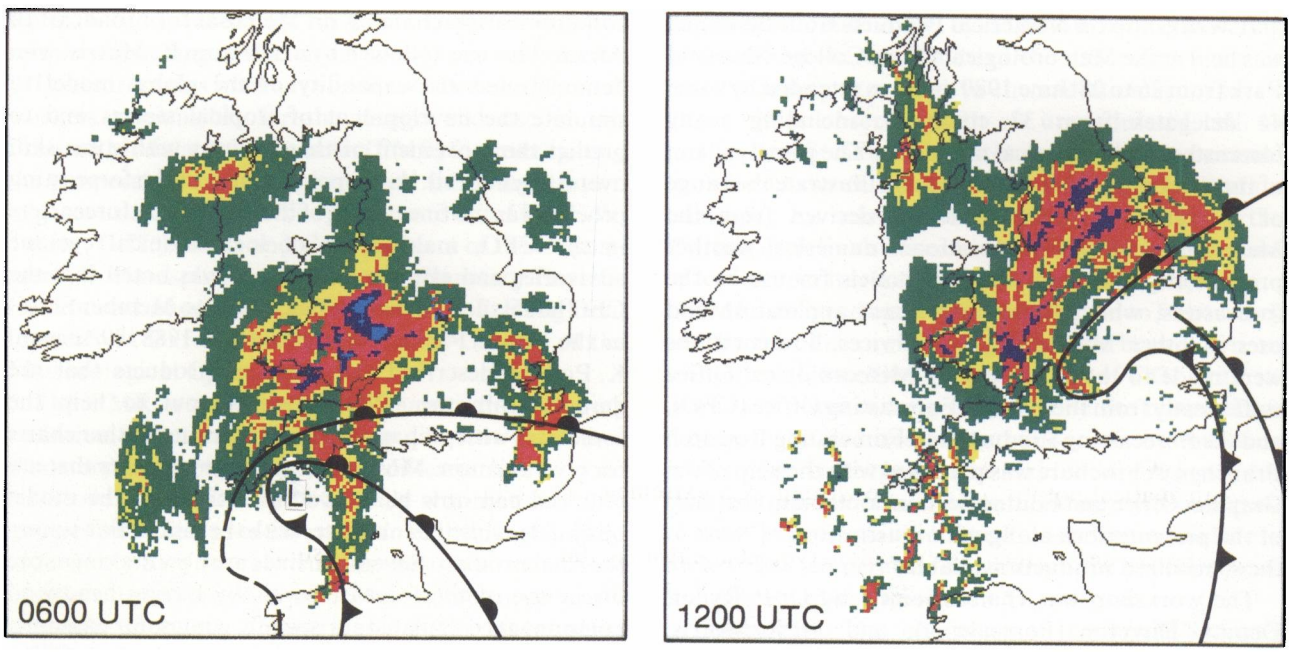

Figure 1. Radar pictures for 0600 and 1200 UTC on 8 November 1989. Increasing rainfall rates are represented by the colour sequence: green, yellow, red, magenta, blue and cyan. Frontal locations are superimposed, dashed where uncertain.

The major feature in the pictures is a broad band of rain to the north of and curving around the western flank of an intense deepening low. Sequential replay of images indicated that the precipitation pattern as a whole moved with the low, although individual precipitation elements within its western flank turned cyclonically and quickly decayed. The rain-bands over south-east England and the English Channel at 0600 UTC moved quickly north-eastwards and by 1200 UTC convection was occurring over south-west England (Fig. 1).

The surface frontal analysis is particularly interesting. Detailed analysis of temperature and dew-point (Fig. 2) suggests the double structure shown. The strongest thermal gradient is associated with the northern warm front, which is related to the major rain area and is bent back around the low centre, where there is a small warm core. There is no evidence of occlusion. By 1200 UTC, it was difficult to locate two cold fronts.

The overall distribution of precipitation and surface weather was similar to that of several other intense depressions, including the storm of October 1987. In each case a bent back warm front* could be analysed which was very active in terms of thermal contrast and precipitation with very low temperatures observed in the area of heavy rain to the north. Behind the low (usually on the western flank), precipitation decayed rapidly. Strongest winds within each cyclonic system lay within and just ahead of the region of precipitation decay.

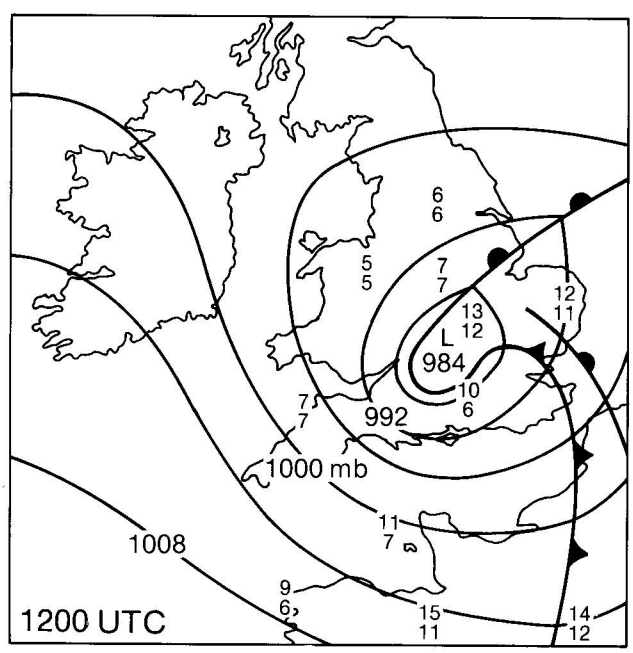

Figure 2. Surface analysis at 1200 UTC on 8 November 1989. Temperatures (°C) (upper) and dew-points (lower) are shown for selected observing stations.

G.A. Monk

* Shapiro, M.A. (1989) The mesoscale structure of extratropical marine cyclones. IAMAP 1989. Abstracts, Vol. 2.

GUIDE TO AUTHORS

Content

Articles on all aspects of meteorology are welcomed, particularly those which describe results of research in applied meteorology or the development of practical forecasting techniques.

Preparation and submission of articles

Articles, which must be in English, should be typed, double-spaced with wide margins, on one side only of A4-size paper. Tables, references and figure captions should be typed separately. Spelling should conform to the preferred spelling in the *Concise Oxford Dictionary* (latest edition). Articles prepared on floppy disk (Compucorp or IBM-compatible) can be labour-saving, but only a print-out should be submitted in the first instance.

References should be made using the Harvard system (author/date) and full details should be given at the end of the text. If a document is unpublished, details must be given of the library where it may be seen. Documents which are not available to enquirers must not be referred to, except by 'personal communication'.

Tables should be numbered consecutively using roman numerals and provided with headings.

Mathematical notation should be written with extreme care. Particular care should be taken to differentiate between Greek letters and Roman letters for which they could be mistaken. Double subscripts and superscripts should be avoided, as they are difficult to typeset and read. Notation should be kept as simple as possible. Guidance is given in BS 1991: Part 1: 1976, and *Quantities, Units and Symbols* published by the Royal Society. SI units, or units approved by the World Meteorological Organization, should be used.

Articles for publication and all other communications for the Editor should be addressed to: The Director-General, Meteorological Office, London Road, Bracknell, Berkshire RG12 2SZ and marked 'For Meteorological Magazine'.

Illustrations

Diagrams must be drawn clearly, preferably in ink, and should not contain any unnecessary of irrelevant details. Explanatory text should not appear on the diagram itself but in the caption. Captions should be typed on a separate sheet of paper and should, as far as possible, explain the meanings of the diagrams without the reader having to refer to the text. The sequential numbering should correspond with the sequential referrals in the text.

Sharp monochrome photographs on glossy paper are preferred; colour prints are acceptable but the use of colour is at the Editor's discretion.

Copyright

Authors should identify the holder of the copyright for their work when they first submit contributions.

Free copies

Three free copies of the magazine (one for a book review) are provided for authors of articles published in it. Separate offprints for each article are not provided.

January 1990

Editor: B.R. May
Editorial Board: R.J. Allam, R. Kershaw, W.H. Moores, P.R.S. Salter

Vol. 119
No. 1410

Contents

Contributions: It is requested that all communications to the Editor and books for review be addressed to the Director-General, Meteorological Office, London Road, Bracknell, Berkshire RG12 2SZ, and marked 'For *Meteorological Magazine*'. Contributors are asked to comply with the guidelines given in the *Guide to authors* which appears on the inside back cover. The responsibility for facts and opinions expressed in the signed articles and letters published in *Meteorological Magazine* rests with their respective authors. Authors wishing to retain copyright for themselves or for their sponsors should inform the Editor when submitting contributions which will otherwise become UK Crown copyright by right of first publication.

Subscriptions: Annual subscription £30.00 including postage; individual copies £2.70 including postage. Applications for postal subscriptions should be made to HMSO, PO Box 276, London SW8 5DT; subscription enquiries 01–873 8499.

Back numbers: Full-size reprints of Vols 1–75 (1866–1940) are available from Johnson Reprint Co. Ltd, 24–28 Oval Road, London NW1 7DX. Complete volumes of *Meteorological Magazine* commencing with volume 54 are available on microfilm from University Microfilms International, 18 Bedford Row, London WC1R 4EJ. Information on microfiche issues is available from Kraus Microfiche, Rte 100, Milwood, NY 10546, USA.

ISBN 0 11 728661 3

ISSN 0026–1149

Printed in the United Kingdom for Her Majesty's Stationery Office
Dd 0291241 1/90 C13 503 12521